TopoWellPlate

TopoWellPlate: A Well-Plate-Based Screening Platform to Study Cell–Surface Topography Interactions

*Nick R. M. Beijer, Aliaksei S. Vasilevich, Bayram Pilavci, Roman K. Truckenmüller, Yiping Zhao, Shantanu Singh, Bernke J. Papenburg, and Jan de Boer**

The field of biomaterial engineering is increasingly using high-throughput approaches to investigate cell–material interactions. Because most material libraries are prepared as chips, immunofluorescence-based read-outs are used to uniquely image individual materials. This paper proposes to produce libraries of materials using a well-based strategy in which each material is physically separated, and thus compatible with standard biochemical assays. In this work, the TopoWellPlate, a novel system to study cell–surface topography interaction in high-throughput is presented. From a larger library of topographies, 87 uniquely defined bioactive surface topographies are identified, which induce a wide variety of cellular morphologies. Topographically enhanced polystyrene films are fabricated in a multistep cleanroom process and served as base for the TopoWellPlate. Thermal bonding of the films to bottomless 96-well plates results in a cell culture ready, topographically enhanced, 96-well plate. The overall metabolic activity of bone marrow-derived human mesenchymal stem cells is measured to show the functionality of the TopoWellPlate as a screening tool, which showed a 2.5-fold difference range in metabolic activity per cell. TopoWellPlates of this and other topographical designs can be used to analyze cells using the wealth of standardized molecular assays available and thus disclose the mechanisms of biomaterials-induced mechanotransduction.

Biomaterials can be engineered to alter cell behavior, often by impinging on mechanotransduction signaling pathways, resulting in phenotypic changes such as in cell morphology and alignment, migration, proliferation rates, and directed cell fate.[1–3] The influence of individual material parameters on cell behavior is widely studied, often by modifying one property of the biomaterial. For example, substrate surface chemistries can be varied, from synthetic polymers to biomolecules[4,5] and bulk material properties such as degradability and elasticity can be modified. Furthermore, microcontact printing is used to change the size and shape of cell adhesive islands. In a seminal paper, Chen et al. showed that apoptosis and proliferation of endothelial cells can be controlled by altering the size of the adhesive island on which the cell grows.[6] Using a similar approach, the same group demonstrated a role for Rho-mediated signaling in the control of adipogenic and osteogenic differentiation. Another relation between a biomaterial property and cellular response is reported by Swift et al. who demonstrated that extra cellular matrix stiffness correlates to lamin-A conformation and expression levels.[7]

In these, and most other cases, only a very limited part of the full biomaterial design space is covered. Moreover, in most cases, a relation is found between material properties and a phenotypical read-out, but the complex molecular mechanisms linking this material property to the change in phenotype is largely unknown. To address this, state-of-the-art high-throughput platforms are used. These systems serve as excellent starting points to identify materials which are able to induce desirable cell behavior. Comparable to low-throughput work, high-throughput systems are used to explore material properties such as bulk material chemistry,[8,9] surface chemistry,[10] and surface structure. Here, primarily imaging-based read-outs are used to screen for one biomarker in the desired phenotype because the material libraries are spotted onto glass slides or produced as arrays on chemically nonseparated sheets. For example, three different platforms are used nowadays to screen for bioactive surface topographies in high-throughput: multiarchitecture chip (MARC, consisting of isotropic/anisotropic, nano- and micrometer scale, polydimethylsiloxane

N. R. M. Beijer, A. S. Vasilevich, B. Pilavci, Prof. J. de Boer
Department of Cell Biology Inspired Tissue Engineering
MERLN Institute for Technology-Inspired Regenerative Medicine
Maastricht University
Universiteitssingel 40, Maastricht 6229 ER, The Netherlands
E-mail: jan.deboer@maastrichtuniversity.nl
Dr. R. K. Truckenmüller
Department of Complex Tissue Regeneration
MERLN Institute for Technology-Inspired Regenerative Medicine
Maastricht University
Universiteitssingel 40, Maastricht 6229 ER, The Netherlands
Dr. Y. Zhao, Dr. B. J. Papenburg
Materiomics BV
Oxfordlaan 70, Maastricht 6229 EV, The Netherlands
Dr. S. Singh
Imaging Platform
Broad institute of MIT and Harvard
415 Main street, Cambridge, MA 02142, USA

DOI: 10.1002/adbi.201700002

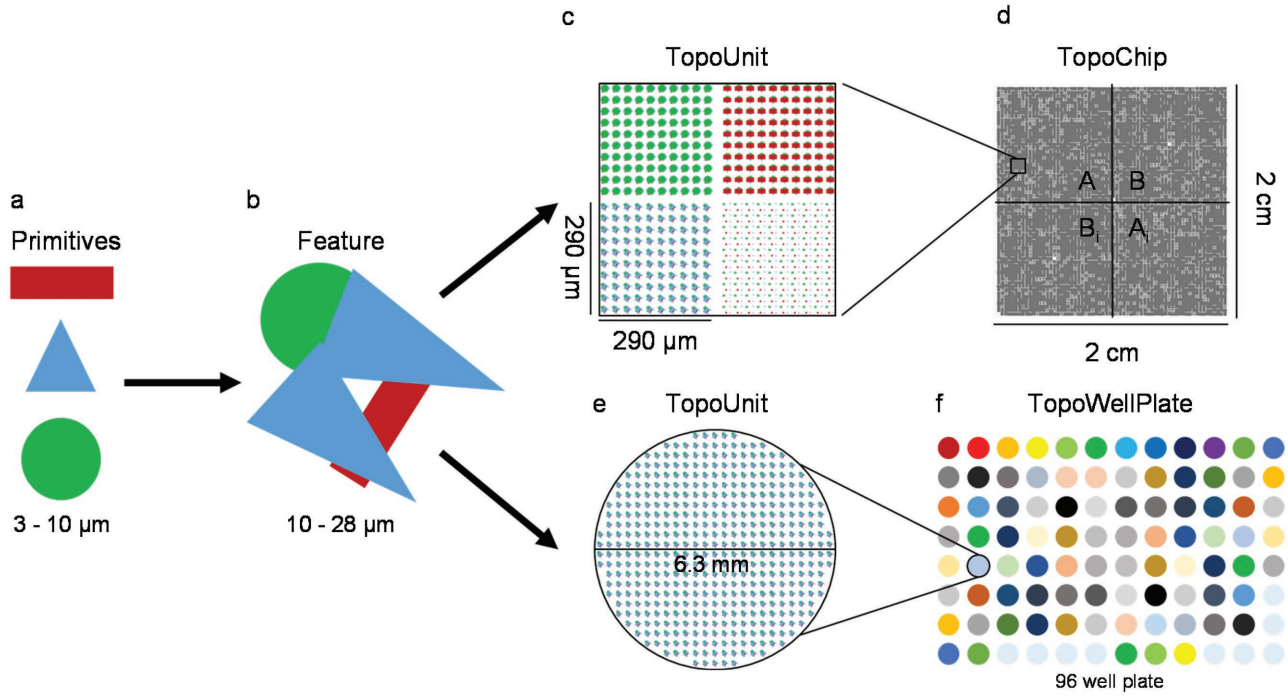

Figure 1. TopoWellPlate as a new member of the TopoChip platform. a) Primitive shapes (namely, circles, triangles, and rectangles) are used to design b) topographical features. Arrays of a unique topographical feature build c) a 290 × 290 µm square TopoUnit for d) the TopoChip and e) an isolated circular TopoUnit of 6.3 mm in diameter for f) the TopoWellPlate. The TopoChip contains 2176 unique surface topographies in duplicate and 4 unpatterned units, whereas the TopoWellPlate contains 87 unique surface topographies and 9 unpatterned wells.

(PDMS) surface topographies),[11] biosurface structure array (BSSA, consisting of topographical features designed using a combinatorial approach of lateral and vertical dimensions),[12] and the TopoChip.[13] Using MARC, Moe et al. identified a surface structure able to enhance neural differentiation of primary murine neural progenitor cells.[11] Lovmand et al. used the BSSA to identify surface structures that enhanced mineralization as well as the expression of osteogenic markers of a pre-osteoblastic murine cell line.[12]

On the TopoChip, defined surface structures are created by combining circles, squares, and rectangles (**Figure 1**a) into topographical features (Figure 1b) that vary in size, density, and roundness. These topographical features are placed in an arrayed order in 290 × 290 µm TopoUnits (Figure 1c). In total 2176 TopoUnits with unique surface topographies are placed in duplicate on a 2 × 2 cm polymer cell culture tool, designated the TopoChip (Figure 1d). We observed dramatic changes in cell and nuclear morphologies correlating to the topographical feature design parameters.[14] In present—more application-driven—work, we identified a bioactive surface that can be used to improve the lifespan of orthopedic implants. Here, surface topographies are selected that induced osteogenesis in vitro and increased bone bonding in vivo (manuscript submitted). Furthermore, a set of specific topographical features is identified which maintained the expression levels of the pluripotency markers OCT4 and SOX2, and thus overcomes difficulties in xeno-free induced pluripotent stem cell (IPSC) culture.[15]

As most other high-throughput screening systems, the TopoChip relies on imaging-based read-outs as it is difficult to address individual TopoUnits differently. However, the study of topography-induced cellular responses could greatly benefit from the realm of molecular biology techniques available, such as RNA sequencing, enzyme-linked immunosorbent assays (ELISA), mass spectrometry, or other biochemical assays. To be able to do so, the cell cultures should meet two criteria; the populations exposed to a unique surface topography should be isolated, and should be large enough to retrieve sufficient amounts of biological material. In order to validate screening results, selected hit topographies are further assessed in low-throughput on larger, isolated replicates. So far, this led to valuable insights in cell–surface topography interaction such as the regulation of chondrogenic differentiation marker genes in ATDC5 cells[16] and M1/M2 differentiation of macrophages observed during different phases (manuscript inpreparation). Upscaling of topographically enhanced materials is a costly and time consuming process, which raises the urge for a system to study a wide range of surface topographies, and which has compatibility with standard well plate technologies. A few platforms are available for screening cell–material interactions in a well plate format. Zant and Grijpma designed a method to screen hydrogel properties for their influence on cell attachment and proliferation. Synthesizing 255 different hydrogels in 96-well plates allowed them to quickly assess the individual populations by collecting culture medium and cell lysates.[9] A second example is described by Yang et al. who studied the influence of inorganic additives in calcium phosphates on behavior of osteoblasts and osteoclasts in a screening manner.[17] Hu et al. introduced a PDMS-based platform to test the influence of multiple

grid and grating conformations in combinations with drugs on T cell activity. Using this combinatorial approach, they were able to identify both IL-2 secretion enhancing and suppressing cell microenvironments.[18]

In this work, we present the TopoWellPlate, a screening tool for bioactive surface topographies which allows in-depth analysis of the involved molecular mechanisms. The TopoWellPlate consists of 87 isolated TopoUnits displayed over larger areas of surface in the well base (Figure 1e,f). Furthermore, the supervised machine learning approach to select the surface topographies as well as the multistep cleanroom process are described in detail. To show the functionality of the TopoWellPlate, we measured the metabolized cell culture medium of the individual cell populations and observed a wide range of cellular reactions to the surface topographies.

To study cell–material interactions by systematic screening using techniques other than immunocytochemistry, we developed the TopoWellPlate. Clearly, the TopoWellPlate had to resemble a normal tissue culture 96-well plate, as a leakage-free system without cytotoxic chemical contamination of the cell culture environment. A supervised machine learning algorithm was used to select 87 defined surface topographies in order to create a large diversity in cell morphologies on the TopoWellPlate. From the original image database of human mesenchymal stromal cells (hMSCs) on a titanium-coated TopoChip (manuscript submitted) we selected five distinct cell morphologies. These particular morphologies were eye-catching during unautomated image analysis and intuitively labeled as "pancakes," "stretched pancakes," "sticks," "multipolar," and "branched" (**Figure 2**a). Images corresponding to the defined cell morphologies were then introduced (supervised) to an algorithm to create binary classifiers for each morphological group (Figure 2b). Assessing the complete library of images using the obtained binary classifiers allowed us to select multiple unique surface topographies which induced similar cell morphologies. The percentage of cells classified as the desired morphology per image was a measure for the robustness with which the surface topography induced this particular cell morphology. The surface topographies included in the TopoWellPlate were all selected based on this robustness (data not shown). Additionally, we included topographies inducing three different classes of nuclear morphologies as well as three classes of extreme cell morphologies that were rarely—however robustly—observed. We confirmed a great resemblance of cell morphologies when comparing the original images from the TopoChip database with the cells cultured in the TopoWellPlate (Figure 2c). With this, we created the TopoWellPlate consisting of 87 wells with unique surface topographies, which will induce 11 distinct classes of cellular and nuclear morphologies in a very reproducible manner, and 9 wells which remain without any surface topography.

The fabricated polystyrene films with the selected topographies distributed to cover the surface areas under the chimneys of a bottomless 96-well plate, were cropped to exactly fit the bottom region of the well plates. Prior to thermal bonding, the bottomless well plates and the two topography enhanced films were aligned. Applying 108 °C and 6.4 MPa for 45 s resulted in tightly sealed wells, and by this, a ready-to-use cell culture

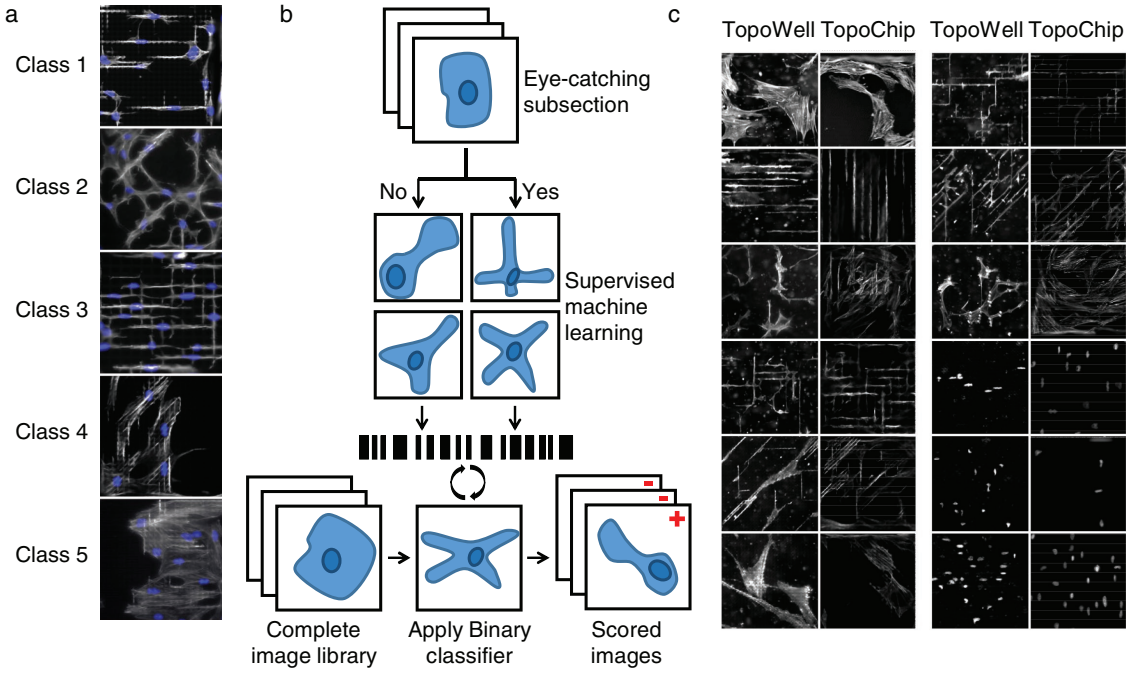

Figure 2. Robust clustering of cellular morphologies. Fluorescence images, obtained in a high-throughput TopoChip screen, were used to identify a) five distinct cell morphologies to perform binary classification. b) The classifiers obtained by supervised machine learning in CellProfiler Analyst were able to classify cells based on morphology with at least 70% accuracy. c) Testing the complete library of images with the binary classifiers let to the identification of multiple surface topographies able to induce the desired described cell morphologies, and in addition extreme morphologies (both cellular and nuclear) found to occur on fewer occasions. All described classes were scattered on the design of the TopoWellPlate.

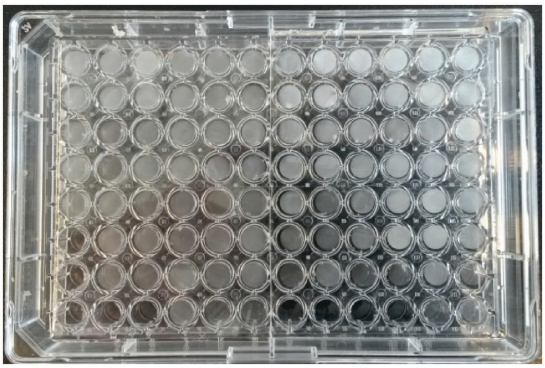

Figure 3. The TopoWellPlate. The thermal bonding of the topographically enhanced polystyrene film and the bottomless 96-well plate, results in a leakage free well plate containing high-quality defined surface structures.

system (**Figure 3**). Here, neither the polystyrene base material nor the thermal bonding process caused changes in cell viability when compared to standard cell culture plates. And visual inspection of the topographical features showed high-quality defined surface structure over the entire area of the wells before, during and after cell culture (data not shown).

The TopoWellPlate is envisioned to be used as high-throughput system to study the influence of surface topography on cell behavior with nonimaging-based techniques. To show this potential, we performed a biochemical assay on the culture medium of all individual TopoUnits. Here, we measured the overall metabolic activity of hMSC populations exposed to the 87 defined surface topographies and the populations on the unpatterned references. The Presto Blue assay used measures the conversion of the nonfluorescent resazurin into the highly fluorescent resorufin. This conversion takes mainly place in the reducing environment of mitochondria where NADPH/NADH (nicotinamide adenine dinucleotide phosphate/nicotinamide adenine dinucleotide) dehydrogenase creates the reductant NADPH/NADH. Fluorescence intensities measured in the Presto Blue assay thus represent the mitochondrial metabolic activity. **Figure 4**a shows the distribution of resazurin conversions in cell populations exposed to unique surface topographies. We observed a clear 2.5 times difference between the lowest and highest scoring populations (Figure 4b) and remarkably, cell populations grown in unpatterned wells were all among the highest scoring populations. This demonstrated the diversity in physical stimuli on the TopoWellPlate and its influence on cell behavior.

In this work, we have introduced the TopoWellPlate as a valuable tool to study cell–material interaction in a high-throughput manner. We established the TopoWellPlate production flow and set-up cell culture protocols that resemble the standard well plate cell culture systems. Our growing database on the bioactivity of surface topographies from the TopoChip platform in combination with the used fabrication pipeline has great potential for further development. First, the surface topographies included in the current design of the TopoWellPlate can be replaced by any other topography available in our in silico library. Besides the selection of topographies on the current TopoWellPlate, which is known to induce a wide variety of cell morphologies, one could, for example, include a selection of topographies that cover the full spectrum of a single design parameter for the topographical features. Second, the current 96-well plate design can be transformed into 384 and even 1536-well formats to cover the range of topographical features even more comprehensively. Third, recent data showed the ability to scale topographical feature sizes down from micrometer to nanometer scale while maintaining the high topographical feature structures quality and reproducibility (manuscript submitted). Furthermore, it is shown that the effect of surface topography on cell behavior is strongly influenced by bulk material chemistry.[19] One specific combination of surface topography, material chemistry, and cell type will give a unique result, and therefore, we foresee the use of the TopoWellPlate of various materials to study many more mechanobiologically relevant models. To add another layer of complexity, well-plate-based system can be developed in which a defined 3D cell culture is created. Multiple platforms are

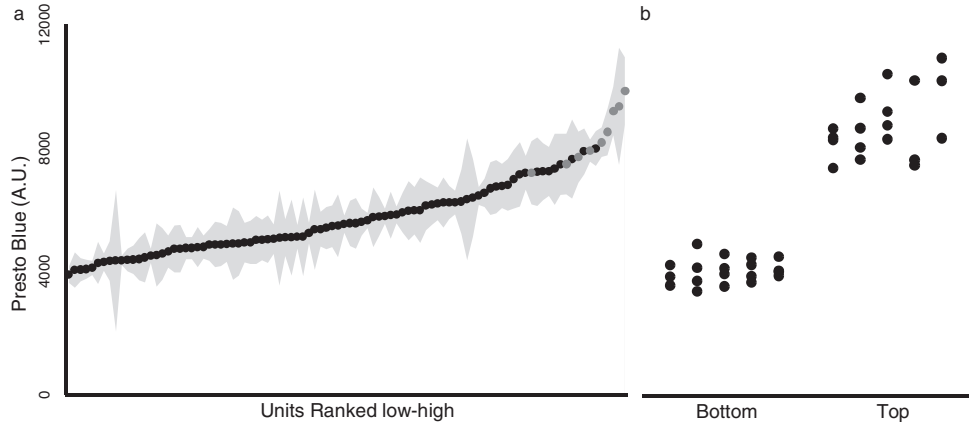

Figure 4. Topography induced changes in metabolic activity of cells cultured on different topographies in the TopoWellPlate. Metabolic activity of hMSC populations in the TopoWellPlate exposed to 87 unique surface topographies and 9 unpatterned surfaces for 3 d measured using Presto Blue. a) Each dot represents the average metabolic activity for a cell population cultured on a single unique surface topography ($n = 4$) (topographically enhanced TopoUnits represented by black dots, unpatterned TopoUnits by dark gray, and the light gray fields above and below the dots represents the standard deviation), and is ranked from low to high. b) Raw data points of the top and bottom scoring units.

used to study the influence of an engineered 3D microenvironment on cell behavior. For example, Ma et al. used a bioprinting approach to create arrays of 3D cell laden hydrogels with gradients of extra cellular matrix components able to alter cell behavior of periodontal ligament stem cells.[20] Using rapid prototyping, Higuera et al. created defined 3D structures of biomaterials in wells which allowed them to study the influence of the construct in higher throughput both in vitro and in vivo.[21]

The proof of principle described in this work shows the diversity in cellular responses to surface topography as measured by the cells their mitochondrial metabolic activity. With mitochondria as the main energy producing cell organelles, one can hypothesize that changes in mitochondrial abundance occur induced by surface topography. The dramatic changes in cell morphology—observed on the TopoWellPlate–are accompanied by changes in cell size. With this, a proportionate decrease in cell organelles as mitochondria in smaller cells is possible.[22] Furthermore, the cell metabolism can be divided in multiple pathways, and the TopoWellPlate allows us to investigate the effect of surface topography on these pathways in depth.

The use of different omics approaches on the TopoWellPlate is in line with our current high-throughput approach. In particular, transcriptomic profiling using the L1000 technology allows us to create a gene expression dataset on cell–material interaction which is unique to our knowledge.[23] Besides standard gene expression data analysis techniques focusing on differentially expressed genes and their functions, other types of analysis offer interesting opportunities for further research. For example, our transcriptomic data could be used for analysis in the Connectivity Map which allows for a comparison of the biomaterial-induced gene expression profile with small molecule-induced profiles.[24] In addition, our data can be placed in the compendium for biomaterial transcriptomics (cBiT), which accumulates biomaterial-based transcriptomics studies along with a detailed characterization of the biomaterial properties, making comparisons with similar materials possible (https://cbit.maastrichtuniversity.nl). However, besides transcriptomics, many other techniques can be used to obtain valuable information. The TopoWellPlate allows us to study surface topography induced cytokine secretion by the multiplex ELISA, and to create proteomic and metabolomics profiles using mass spectrometry.

Recently, the number of mechanobiologically relevant cell systems has been growing and future applications of defined bioactive surface topographies can be introduced here. We aim to target a wide variety of biological models in which mechanical stimuli might play an important role. For example, corneal endothelium regeneration,[25] macrophage stimulation,[26] activation of the immune responses in mesenchymal stromal cells,[27] and tailoring the epigenetic state of cells.[28] We also aim to improve standard cell culture protocols by developing culture plates that overcome current limiting factors. For example, IPSC maintenance[5] and differentiation,[29] the loss of stemness in stem cell cultures, increase proliferation rates for slow growing cell types, disrupting colony formation, and stimulating monolayer formation. We recently identified a surface topography able to maintain primary hepatocytes viable during prolonged periods of in vitro cell culture (work progress). Including only this specific topography in a TopoWellPlate system allows us to screen libraries of small molecules for drugs discovery in this engineered biological model.

To conclude, the TopoWellPlate allows us to compile large datasets on various levels of cell behavior that can be used to uncover the "big black box" of signaling cascades in mechanobiology. This knowledge will help us to elucidate the full underlying mechanism of mechanotransduction in mechanobiologically relevant models.

Experimental Section

Topography Selection: Bone marrow derived hMSCs cultured for 5 d under basic conditions on eight titanium coated poly-lactic-acid TopoChips were fluorescently stained for DNA (DAPI, Life Technologies), actin cytoskeleton (phalloidin, Life Technologies), and osteogenic differentiation related protein alkaline phosphatase (ALP, sc137213, Santa Cruz Biotech). High content imaging of the cells on the TopoChips was performed using the BD pathway. The 2176 unique surface topographies (duplicates per chip) and the nonpatterned TopoUnits (four replica's per chip) were captured in individual images of all eight TopoChips. Prior to image analysis, a variety of image correction steps were performed which included: region of interest (ROI) cropping, alignment, and background signal removal.

Image analysis was performed using CellProfiler.[30] After segmentation of individual cells in the ROI, a 1000 node cluster analysis was performed. With this datasets on most morphological parameters were obtained that are available in the CellProfiler software. Subsequently, CellProfiler analyst 2.0,[31] a tool for supervised machine learning analysis relying on a gently boosting algorithm, was used to explore the variety of cell morphologies in the TopoChip data. To initiate this algorithm, five eye catching cell morphologies were selected from the image database. Subsequently, CellProfiler analyst was used to create the five corresponding binary classifiers. Here, at least 100 cells per morphological cluster were presented to the program in order to create a classification accuracy of 70%. The obtained binary classifiers (features used in these classifiers are shown in **Table 1**) were then used to assess the complete dataset, where all images (corresponding to one TopoUnit) were scored based on the percentage of cells that belong to one of the defined classifiers. The most frequent TopoUnits in the 1000 highest scored images were selected as surface topography inducing one of the five classified cell morphologies in a robust and reproducible way.

Topography Enhanced Polystyrene Film Fabrication Process: Patterns of the selected surface topographies were placed in a 96-well plate format as the lay-out of the chromium masks for photolithography. The micrometer-scale patterns were etched from the silicon wafer by directional reactive ion etching (DRIE), generating a silicon master

Table 1. Binary classifier parameters for five cellular morphologies. (CellProfiler analyst supervised machine learning on five distinct cell morphologies led to the description of corresponding binary classifiers. The rules for classification are based on few morphological parameters all with a different weight in the classification process. Here, orange shading represents morphological parameters important in the binary classifying process with an accuracy of 70%, green parameters of medium importance, and blue of low importance.)

Class 1	Class 2	Class 3	Class 4	Class 5
Eccentricity	Area	Solidity	Eccentricity	Area
Compactness	Minor axis	Eccentricity	Area	Compactness
Neighbors	Solidity	Area	Solidity	
Minor axis	Extent			

mould. Due to wafer size limitations, two moulds were needed to create a lay-out with the size of a 96-well plate. These silicon master moulds contained the inverse topography patterns. A three-replication process was used to fabricate the surface topography enhanced polystyrene films.[32] In these three replications, silicon moulds, PDMS moulds, and Ormostamp moulds were subsequently used.

Silicon Master Mould Fabrication: Si ⟨100⟩ wafers were prepared with positive photoresist (907-16, Olin) by spin-coating at 4000 rpm for 30 min. The prepared substrates were patterned using the designed masks in conventional UV lithography (EVG 620). After development (OPD 4262) and hard baking on a hotplate at 120 °C for 30 min, the wafers were etched by DRIE (Adixen AMS 100 SE) using a Bosch process of SF6/C4F8 flow of 250/200 sccm (3/1 s), ICP of 1500 W, CCP of 80 W, and a substrate temperature of 80 °C for 3 min and 18 s. By this, a feature depth of 10 µm was obtained. The photoresist was then stripped in O_2 plasma.

PDMS Mould Fabrication: The silicon master moulds (**Figure 5**a) were first cleaned in Piranha solution (H_2SO_4: H_2O_2 = 3:1 v/v) for 30 min at 95 °C, rinsed with deionized water, spun dried with N_2, and coated with a monolayer of trichloro(1H, 1H, 2H, 2H-perfluorooctyl)silane (FOTS, Sigma-Aldrich) in the gas phase under vacuum in a desiccator. Degassed PDMS (curing agent: base = 1:10 w/w, Sylgard 184 silicone elastomer kit, Dow Corning Corporation) was casted (Figure 5b) on the full 100 mm silicon master mould to create a 1–2 mm thick PDMS mould, and cured on a leveled hotplate at 80 °C for at least 8 h (Figure 5c). After curing, the PDMS film was peeled from the silicon mould (Figure 5d) and ready to be used for the next replication cycle.

Ormostamp Mould Fabrication: Due to thermal expansion and mechanical properties of PDMS, the obtained PDMS mould could not be used as a proper template for hot embossing. Therefore, a second replication step was needed using a much harder polymer. For this, Ormostamp (OrmoStamp, Micro Resist Technology GmbH, Germany), a UV-curable inorganic–organic hybrid polymer was used. A layer of Ormoprime (OrmoPrime08, Micro Resist Technology GmbH, Germany) was applied on a clean support Borofloat wafer (Borofloat 33 of 100 mm diameter and 500 µm thickness from Schott) via spin-coating for 30 s at 4000 rpm followed by 5 min on a hot plate at 150 °C. This layer promoted adhesion of the Ormostamp and was prepared immediately before application. 1.5 mL Ormostamp was slowly dispensed in the middle of the PDMS mould (Figure 5e) and carefully brought into contact with the Borofloat wafer with the Ormoprime coating. The gap between the two substrates was completely filled by capillary force after 30 min (Figure 5f). The PDMS/Ormostamp/Borofloat sandwich was exposed to 365 nm UV light for 300 s with a light intensity of 12 W cm^{-2} (EVG 620 i-line exposure system) (Figure 5g), after which the PDMS mould was peeled from the Ormostamp mould (Figure 5h). UV curing was followed by a hard bake process on a hot plate at 130 °C for 30 min (ramping up from room temperature at a ramping speed of 5 °C min^{-1}) to finalize this replication cycle.

Polystyrene Hot Embossing: Before the third replication step, the Ormostamp mould was treated with a gentle O_2 plasma (reactive ion etching (home-build) at 10 °C, 50 sccm oxygen flow, 75 mTorr pressure, and 50 W CCP power for 30 s) and FOTS coated as described earlier (Figure 5i). Commercially available biaxially oriented 190 µm thick polystyrene films (Goodfellow, United Kingdom) were used as substrate material (Figure 5j) for hot embossing (Obducat Eitre6 Nano Imprint Lithography system, Obducat, Sweden) the inverse ORMO stamp template at 140 °C and 10 bars for 5 min (Figure 5k). The replication process was finalized by separating the Ormostamp template from the 10 µm high topographical features enhanced polystyrene films at 95 °C (Figure 5l). To improve cell adhesion in the later stages of the project, a gentle O_2 plasma treatment was applied as described above.

TopoWellPlate Assembly: Size adjustment of both produced films was needed before substrate alignment for thermal bonding. Here, the

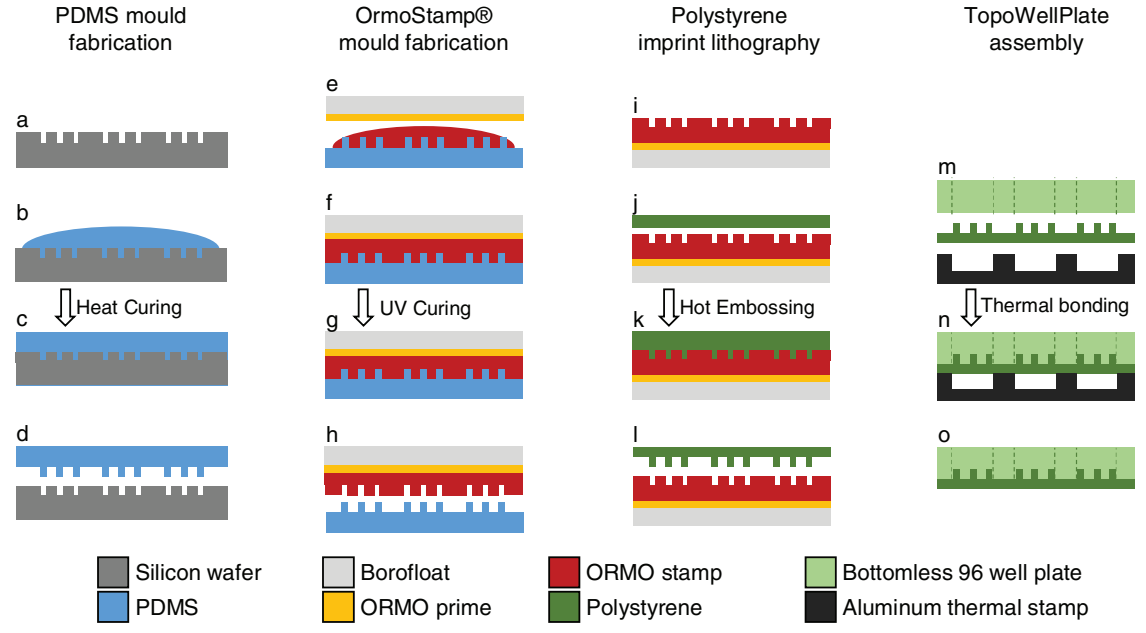

Figure 5. Fabrication scheme of PDMS and Ormostamp moulds and hot embossing of topography enhanced polystyrene films. The process of creating the topography enhanced polystyrene films for the TopoWellPlate consists of the following steps (see the Experimental Section for a more in depth description): a) Silicon master mould containing the inverse structures of the selected topographies used to b) cast a layer of PDMS followed by c) the curing of the PDMS layer and d) peeling it off the silicon master. e) OrmoPrime08 is applied to a Borofloat wafer and application of Ormostamp on the PDMS copy, f) spreading by capillary forces, g) UV curing, and h) peeling off the Ormostamp mould. The hot embossing process starts with i) the inverse Ormostamp mould, j) aligning the polystyrene film and the mould, k) hot embossing, and finally l) gently peeling it off the topographically enhanced film used as bottom for the TopoWellPlate. Assembling the TopoWellPlate starts by m) aligning the bottomless 96-well plate, topographically enhanced polystyrene film and aluminum thermal stamp, followed by n) thermal bonding at 108 °C and 6.4 MPa for 45 s, resulting in o) a leakage-free well plate containing high-quality defined surface structures.

topographically enhanced areas of the polystyrene films were exactly aligned (Figure 5m) with the chimneys of a bottomless 96-well plate (Greiner Bio-One) and an in-house developed aluminum controlled heat transmitting stamp. The stack was placed in a temperature-controlled press where the temperature of the well plate was increased to 50 °C and the aluminum stamp to 108 °C for 4 min, followed by 45 s at a compression pressure of 6.4 MPa (Figure 5n) and demolding immediately afterward (Figure 5o). This resulted in a polystyrene 96-well plate with 87 wells that were enhanced with a surface topography and 9 wells that remained unpatterned.

Cell Culture: A bone marrow aspirate was obtained from a donor (D210, female/74 years old) who was undergoing a total hip replacement surgery and had given informed consent. In the aspirate, the nucleated cells were counted and plated at a density of 500 000 cells cm^{-2} in hMSC proliferation medium which consists of basic medium (a-minimal essential medium (a-MEM, Life Technologies), 10% fetal bovine serum (Sigma), 0.2×10^{-3} M ascorbic acid (Sigma), 2×10^{-3} M L-glutamine (Fisher Scientific) and 100 units mL^{-1} penicillin with 100 mg mL^{-1} streptomycin (Fisher Scientific)) with an additional 1 ng mL^{-1} basic fibroblast growth factor (Neuromics). Cells were grown at 37 °C, 5% CO_2, and a humidified atmosphere. The hMSCs obtained after the first trypsinization (Trypsin-EDTA (0.05%), Fisher Scientific) were plated at 5000 cells cm^{-2} and considered as passage 1. Basic medium was replaced twice a week and hMSCs were used for expansion, cryopreservation or experiments once 80% confluency was reached. All experiments were performed with passage 5 hMSCs.

Metabolic Activity: The metabolic activity of isolated cell populations exposed to unique surface topographies was measured using the Presto Blue assay (Invitrogen) according to the manufacturer's protocol. In brief, after 3 d basic hMSC culture medium was replaced by Presto Blue medium (1× concentrated in basic hMSC medium), which was incubated with the cell cultures for 1 h at 37 °C in a humid environment. Equal amounts of supernatant were subsequently transferred to a black/black bottom 96-well plate and followed by the quantification of the fluorescent signal measured at 590 nm using a plate reader (Perkin Elmar Victor 3).

Fluorescent Staining and Microscopy: Cells were fixated in freshly prepared 3.7% paraformaldehyde for 10 min at room temperature, permeabilized by 1% Triton-x (Sigma) in phosphate buffered saline (PBS) for 10 min and blocked for a specific binding by 1% bovine serum albumin (Sigma-Aldrich) in PBS for 30 min. The actin cytoskeleton was labeled with phalloidin 488 (1:80, Biotium inc.) for 40 min and the DNA with 4′,6-diamidino-2-phenylindole (DAPI, 14.3×10^{-6} M, Life technologies) for 5 min both in dark and at room temperature. The staining protocol was finalized after multiple washing steps and the samples were kept humid in PBS. Fluorescence images were obtained using the BD pathway.

Acknowledgements

N.R.M.B. and J.dB. gratefully acknowledge the financial support of the European Union's Seventh Framework Program (FP7/2007-2013) STELLAR (Grant Agreement No. 305436). N.R.M.B., A.S.V., and J.dB. acknowledge the financial support of the Dutch province of Limburg. *The authors declare no conflict of interest.*

Received: January 11, 2017
Revised: February 8, 2017
Published online: March 21, 2017

[1] O. Chaudhuri, L. Gu, D. Klumpers, M. Darnell, S. A. Bencherif, J. C. Weaver, N. Huebsch, H.-P. Lee, E. Lippens, G. N. Duda, D. J. Mooney, *Nat. Mater.* **2015**, *15*, 326.

[2] S. Khetan, M. Guvendiren, W. R. Legant, D. M. Cohen, C. S. Chen, J. A. Burdick, *Nat. Mater.* **2013**, *12*, 458.

[3] S. Dupont, L. Morsut, M. Aragona, E. Enzo, S. Giulitti, M. Cordenonsi, F. Zanconato, J. Le Digabel, M. Forcato, S. Bicciato, N. Elvassore, S. Piccolo, *Nature* **2011**, *474*, 179.

[4] M. P. Lutolf, J. L. Lauer-Fields, H. G. Schmoekel, A. T. Metters, F. E. Weber, G. B. Fields, J. A. Hubbell, *Proc. Natl. Acad. Sci. USA* **2003**, *100*, 5413.

[5] K. Saha, Y. Mei, C. M. Reisterer, N. Kenton, J. Yang, J. Muffat, M. C. Davies, M. R. Alexander, R. Langer, D. G. Anderson, R. Jaenisch, *Proc. Natl. Acad. Sci. USA* **2011**, *108*, 18714.

[6] C. S. Chen, M. Mrksich, S. Huang, G. M. Whitesides, D. E. Ingber, C. S. Chen, M. Mrksich, S. Huang, G. M. Whitesides, D. E. Ingber, *Science* **1997**, *276*, 1425.

[7] J. Swift, I. L. Ivanovska, A. Buxboim, T. Harada, P. C. D. P. Dingal, J. Pinter, J. D. Pajerowski, K. R. Spinler, J.-W. Shin, M. Tewari, F. Rehfeldt, D. W. Speicher, D. E. Discher, *Science* **2013**, *341*, 1240104.

[8] Y. Mei, K. Saha, S. R. Bogatyrev, J. Yang, A. L. Hook, Z. I. Kalcioglu, S. W. Cho, M. Mitalipova, N. Pyzocha, F. Rojas, K. J. Van Vliet, M. C. Davies, M. R. Alexander, R. Langer, R. Jaenisch, D. G. Anderson, *Nat. Mater.* **2010**, *9*, 768.

[9] E. Zant, D. W. Grijpma, *Biomacromolecules* **2016**, *17*, 1582.

[10] Y. Y. I. Amin, K. Runager, F. Simoes, A. Celiz, V. Taresco, R. Rossi, J. J. Enghild, L. A. Abildtrup, D. C. E. Kraft, D. S. Sutherland, M. R. Alexander, M. Foss, R. Ogaki, *Adv. Mater.* **2015**, *28*, 1472.

[11] A. A. K. Moe, M. Suryana, G. Marcy, S. K. Lim, S. Ankam, J. Z. W. Goh, J. Jin, B. K. K. Teo, J. B. K. Law, H. Y. Low, E. L. K. Goh, M. P. Sheetz, E. K. F. Yim, *Small* **2012**, *8*, 3050.

[12] J. Lovmand, J. Justesen, M. Foss, R. H. Lauridsen, M. Lovmand, C. Modin, F. Besenbacher, F. S. Pedersen, M. Duch, *Biomaterials* **2009**, *30*, 2015.

[13] H. V Unadkat, K. Cornelissen, B. J. Papenburg, K. Roman, G. F. Post, M. Uetz, J. T. Marcel, D. Stamatialis, C. A. Van Blitterswijk, F. Post, M. J. T. Reinders, *Proc. Natl. Acad. Sci. USA* **2012**, *109*, 5905.

[14] M. Hulsman, F. Hulshof, H. Unadkat, B. J. Papenburg, D. F. Stamatialis, R. Truckenmüller, C. Van Blitterswijk, J. de Boer, M. J. T. Reinders, *Acta Biomater.* **2015**, *15*, 29.

[15] A. Reimer, A. Vasilevich, F. Hulshof, P. Viswanathan, C. A. van Blitterswijk, J. de Boer, F. M. Watt, *Sci. Rep.* **2016**, *6*, 18948.

[16] L. Q. Bach, A. Vasilevich, S. Vermeulen, F. Hulshof, D. Stamatialis, C. A. van Blitterswijk, J. de Boer, *Tissue Eng., Part A* **2016**, DOI: 10.1089/ten.TEA.2016.0421.

[17] L. Yang, S. Perez-Amodio, F. Y. F. Barrère-de Groot, V. Everts, C. A. van Blitterswijk, P. Habibovic, *Biomaterials* **2010**, *31*, 2976.

[18] J. Hu, A. A. Gondarenko, A. P. Dang, K. T. Bashour, R. S. O'Connor, S. Lee, A. Liapis, S. Ghassemi, M. C. Milone, M. P. Sheetz, M. L. Dustin, L. C. Kam, J. C. Hone, *Nano Lett.* **2016**, *16*, 2198.

[19] F. Hulshof, *Ph.D. Thesis*, University of Twente (Enschede), **2016**.

[20] Y. Ma, Y. Ji, G. Huang, K. Ling, X. Zhang, F. Xu, *Biofabrication* **2015**, *7*, 44105.

[21] G. A. Higuera, J. A. A. Hendriks, J. van Dalum, L. Wu, R. Schotel, L. MoreiraTeixeira, M. van den Doel, J. C. H. Leijten, J. Riesle, M. B. J. Karperien, C. A. van Blitterswijk, L. Moroni, *Integr. Biol.* **2013**, *5*, 889.

[22] K. M. Schmoller, J. M. Skotheim, *Trends Cell Biol.* **2015**, *25*, 793.

[23] W. Senkowski, M. Jarvius, J. Rubin, J. Lengqvist, M. G. Gustafsson, P. Nygren, K. Kultima, R. Larsson, M. Fryknäs, *Cell Chem. Biol.* **2016**, *23*, 1428.

[24] J. Lamb, E. D. Crawford, D. Peck, J. W. Modell, I. C. Blat, M. J. Wrobel, J. Lerner, J. Brunet, A. Subramanian, K. N. Ross, M. Reich, H. Hieronymus, G. Wei, S. A. Armstrong, S. J. Haggarty, P. A. Clemons, R. Wei, S. A. Carr, E. S. Lander, T. R. Golub, *Science* **2006**, *313*, 1929.

[25] R. Muhammad, G. S. L. Peh, K. Adnan, J. B. K. Law, J. S. Mehta, E. K. F. Yim, *Acta Biomater.* **2015**, *19*, 138.

[26] K. M. Hotchkiss, G. B. Reddy, S. L. Hyzy, Z. Schwartz, B. D. Boyan, R. Olivares-Navarrete, *Acta Biomater.* **2015**, *31*, 425.
[27] H. Yagi, A. Soto-Gutierrez, B. Parekkadan, Y. Kitagawa, G. Tompkins, N. Kobayashi, M. L. Yarmush, *Cell Transplant.* **2010**, *19*, 667.
[28] T. L. Downing, J. Soto, C. Morez, T. Houssin, A. Fritz, F. Yuan, J. Chu, S. Patel, D. V. Schaffer, S. Li, *Nat. Mater.* **2013**, *12*, 1154.
[29] F. Pan, M. Zhang, G. Wu, Y. Lai, B. Greber, H. R. Schoeler, L. Chi, *Biomaterials* **2013**, *34*, 8131.
[30] A. E. Carpenter, T. R. Jones, M. R. Lamprecht, C. Clarke, I. H. Kang, O. Friman, D. A. Guertin, J. H. Chang, R. A. Lindquist, J. Moffat, P. Golland, D. M. Sabatini, *Genome Biol.* **2006**, *7*, R100.
[31] T. R. Jones, I. H. Kang, D. B. Wheeler, R. A. Lindquist, A. Papallo, D. M. Sabatini, P. Golland, A. E. Carpenter, *BMC Bioinf.* **2008**, *9*, 482.
[32] Y. Zhao, R. Truckenmuller, M. Levers, W.-S. Hua, J. de Boer, B. Papenburg, *Mater. Sci. Eng., C* **2017**, *71*, 558.